Polymer Chemistry

RSC Publishing

PAPER

View Article Online
View Journal | View Issue

Cite this: *Polym. Chem.*, 2013, **4**, 4033

Synthesis and characterization of a low band gap quinoxaline based D–A copolymer and its application as a donor for bulk heterojunction polymer solar cells

M. L. Keshtov,*[a] D. V. Marochkin,[a] V. S. Kochurov,[b] A. R. Khokhlov,[a] E. N. Koukaras[cd] and G. D. Sharma*[ce]

Received 26th March 2013
Accepted 1st May 2013

DOI: 10.1039/c3py00391d

www.rsc.org/polymers

A new alternating copolymer **P** comprising of benzo[1,2-*b*;4,5,*b*′]dithiophene (BDT) derivative and 4,9-bis-(5-bromothiophene-2-yl)-6,7-di-(2-ethylhexyl)-[1,2,5]thiadiazolo[3,4-*g*]quinoxaline (DTQx) derivative electron, donating and electron withdrawing units, respectively, has been synthesized by Stille reaction. The copolymer was characterized by TGA, UV-visible absorption and cyclic voltammetry. The optical band gap of **P** was calculated from the onset wavelength of absorption to be about 1.38 eV. The copolymer **P** was used as electron donor along with $PC_{60}BM$ or $PC_{70}BM$ as electron acceptors for the fabrication of bulk heterojunction solar cells with configurations of ITO/PEDOT:PSS/**P**:$PC_{60}BM$ or $PC_{70}BM$/Al. The power conversion efficiencies (PCE) of the copolymer solar cells blended with $PC_{60}BM$ and $PC_{70}BM$ as electron acceptors, spin cast from THF solvent, were 2.10% and 3.26%, respectively. The PCE device based on the **P**:PC70BM blend processed from DIO/THF was enhanced up to 4.47%. After optimizing the device parameters, such as blend ratio of **P** to PCBM and the choice of processing solvent, power conversion efficiency reaches as high as 5.12% for **P**:$PC_{70}BM$ blend, when processed from DIO/THF solvent, a blend ratio of 1 : 2 w/w and DMSO doped PEDOT:PSS buffer layer is used.

Introduction

Polymer solar cells based on bulk heterojunction (BHJ) active layer, consisting of blends of conjugated polymer donors and fullerene derivative acceptors, are promising sustainable solar energy convertors with various advantages such as flexibility, light weight, large area and low production cost.[1] The active layer of BHJ polymer solar cells forms an interpenetrating network of electron donor and electron acceptor domains.[2] Currently, poly(3-hexylthiophene) (P3HT) is the most widely investigated electron donating material for use in BHJ polymer solar cells and has yielded power conversion efficiencies (PCEs) as high as 5%[3] over the last few years. Li *et al.* have reported PCE of about 5.44%,[4a] 6.5%[4b] and 7.4%[4c] using P3HT as donor and various modified PCBM such as ICBA and $IC_{70}BA$ as electron acceptors. Although P3HT shows excellent charge transfer and separation properties, further improvement in PCE is difficult since it has a relatively high band gap (~1.9 eV) and thus harvests only up to 22% of available photons from the solar light. Moreover, much of the spectral energy is lost by this large difference between the lowest unoccupied molecular orbital (LUMO) levels of P3HT (−3.2 eV) and the fullerene derivatives (−4.0 eV).[3c] Additionally, the high value of the highest occupied molecular orbital (HOMO) (−4.9 eV) limits the open circuit voltage also.[4] To achieve a high PCE, the electron donating polymer must have a band gap smaller than 1.70 eV with LUMO level between −3.5 and −3.7 eV. The difference between the LUMOs of donor polymers and fullerene acceptors must be larger than 0.2–0.3 eV to ensure efficient charge transfer from polymer donor to fullerene acceptor in the BHJ active layer.[5,6] The PCE of solar cells is the product of open circuit voltage (V_{oc}), short circuit current (J_{sc}) and fill factor (FF) of the device under illumination. The J_{sc} is determined by the optical bandgap of the conjugated polymer donor as well as the external quantum efficiency (EQE). The V_{oc} of the BHJ solar cells is directly correlated with the difference between the HOMO of the electron donor polymer and the LUMO of the fullerene acceptor.[7] Therefore, the PCE of BHJ polymer solar cells can be increased by using a low bandgap conjugated polymer while maximizing the energy difference between the HOMO of the donor and LUMO of the acceptor.

[a]*Institute of Organoelement Compounds of the Russian Academy of Sciences, Vavilova st., 28, 119991 Moscow, Russia. E-mail: keshtov@ineos.ac.ru*

[b]*Lomonosov Moscow State University, Faculty of Physics, 1-2 Leninskiye Gory, 119991, Moscow, Russia*

[c]*Institute of Chemical Engineering Science, Foundation for Research & Technology Hellas, Stadiou Str. Platani, Patras, 26504 Greece*

[d]*Molecular Engineering Laboratory, Department of Physics, University of Patras, Patras, 26500, GR, Greece*

[e]*R & D center for Engineering and Science, JEC group of colleges, Jaipur Engineering College campus, Jaipur, 303101 India. E-mail: gdsharma273@gmail.com; sharmagd_in@yahoo.com*

One of the most widely used strategies for obtaining low bandgap conjugated polymers is to design copolymers with alternating electron rich (D; donor) and electron deficient (A: acceptor) units in the backbone.[8] By incorporating a strongly electron donating donor unit and a strongly electron accepting unit in the copolymer backbone, the electronic and optical properties can be tuned. Furthermore, intramolecular charge transfer (ICT) from the D to the A can enhance the π–π stacking between copolymer chains and effectively reduce the bandgap.[9] Several donor–acceptor alternating copolymers with the combination of electron acceptor units such as 2,1,3-benzothiadiazole, thieno[3,4-*b*]pyrazine, quinoxaline, benzo[1,2-*c*,3,4-*c*′]bis[1,2,5]thiadiazole, pyrazino[2,3-*g*]quinoxaline, and [1,2,5]-thiadiazolo[3,4-*g*]quinoxaline or diketo-pyrrolo-pyrrole with various electron donor units have been designed.[10] These copolymers exhibit good PCEs in BHJ polymer solar cells. Although significant progress has been made to reduce the optical bandgap, one major limitation for the PCE enhancement of polymer BHJ solar cells is the low V_{oc}, which is much less than the optical bandgap of the donor polymers.[1a,11] Adding strong electron accepting functional groups is an effective approach to push deeper the HOMO level of the donor polymer without increasing the optical bandgap and thus to increase the V_{oc} of the BHJ polymer solar cells without lowering the J_{sc}.[12]

Quinoxaline (Qx) is a typical electron deficient conjugated unit due to the strong electronegativity of the two nitrogen atoms and relatively stable quinoid form.[13] Many conjugated D–A backbones have been designed using Qx or its derivatives as the electron acceptor unit in their backbones. These Qx-based polymers exhibit interesting photovoltaic effects and PCE ~6% have been reported in the polymers based on thiophene and quinoxaline.[10k,14] Moreover, since Qx consists of two fused six membered rings, when it is copolymerized with other conjugated monomers, the target polymer may have a much lower quinoid property than PBDTTT polymers. Among the wide variety of Qx units, [1,2,5]-thiadiazolo[3,4-*g*]quinoxaline (TQx) has been a promising building block for the synthesis of low bandgap polymers because of the strong electron withdrawing property of the four imine nitrogens in the TQx unit. However, most of the alternating copolymers composed of TQx derivatives as electron acceptor and fluorene or carbazole as electron donor have shown poor photovoltaic performance with a PCE lower than 1%. This low PCE is mainly attributed to the low lying value of the LUMO level of copolymers (−3.9 to −4.0 eV), which is very close to that of PCBM (−4.0 eV). Since the LUMO–LUMO offset between the donor polymer and PCBM should be at least 0.25–0.30 eV, for effective exciton dissociation and charge transfer, a small LUMO–LUMO offset between the TQx based polymers and PCBM may prevent the effective charge separation, which causes the poor PCE.[15] Therefore, it is necessary to raise the LUMO level of the TQx based copolymers in order to promote the charge transfer from the polymer to fullerene and improve the PCE.

In a D–A copolymer, the hybridized LUMO level is located nearly at the LUMO level of the acceptor moiety, while the hybridized HOMO level is governed by the HOMO level of the donor unit.[16] Therefore, to raise the LUMO level of the TQx acceptor unit, an electron donating group should be substituted in the TQx to diminish the electron deficiency of the TQx, thereby weakening the electron affinity of TQx.[16] Recently Chou *et al.* have reported a record PCE of 8.0% for a polymer solar cell with fluorinated quinoxaline based conjugated copolymer PBDT-TFQ as donor and $PC_{71}BM$ as electron acceptor.[17]

Considering the above reasons, we report the synthesis and characterization of a D–A alternating copolymer **P** comprising of benzo[1,2-*b*;4,5,*b*′]dithiophene (BDT) derivative and 4,9-bis-(5-bromothiophene-2-yl)-6,7-di-(2-ethylhexyl)-[1,2,5]thiadiazolo-[3,4-*g*]quinoxaline (DTQx) derivative as electron donating and electron withdrawing units, respectively. The BDT unit, which is a stronger electron donor unit than units such as fluorine or carbazole, assumed an entirely planar and symmetrical structure, thus resulting in high charge mobility. The incorporation of BDT units into DTQx, may have many advantages, such as favoring a planar π–π stacking conformation and a high hole mobility.[18] The optical and electrochemical properties of the copolymer **P** and the performance of the BHJ polymer solar cells based on this copolymer as electron donor and $PC_{60}BM$ or $PC_{70}BM$ are investigated. We have investigated the effects of solvent additive for the blend layer processing and DMSO doping in PEDOT:PSS on the photovoltaic response of the BHJ polymer solar cells. After the optimization of solvent additive concentration for BHJ active layer processing and PEDOT:PSS buffer layer, a PCE of 5.12% has been achieved.

Experimental details, instruments and characterization methods

1H and 13C NMR spectra of the starting compounds and polymers were recorded on the spectrometer "Bruker Avance-400" with working frequencies of 400.13 and 100.62 MHz, respectively. IR spectra were recorded by the FT-IR spectrometer "Perkin-Elmer 1720-X", TGA and DSC analyses were performed on "Perkin-Elmer TGA-7" and "Perkin-Elmer DSC-7" devices with a heating rate of 20 deg min^{-1}.

The absorption spectra in the range 190–1100 nm were recorded on the spectrophotometer "Varian Cary 50". The source of the exciting light was a xenon lamp L8253, which is part of the block radiator with optical fiber output radiation for the "Hamamatsu LC-4". Cyclic voltammetry measurements were performed on a potentiostat-galvanostat μAUTOLAB Type III equipped with standard three-electrode scheme in an acetonitrile solution of 0.1 mol L^{-1} tributylammonium hexafluorophosphate (n-Bu_4NPF_6) at a potential scan rate of 50 mV s^{-1}. Films of the investigated polymers were deposited on a glassy carbon electrode surface and used as working electrode. Ag/Ag^+ and platinum were used as reference and counter electrodes, respectively.

Synthesis of copolymer P

4,7-Dibromo-5,6-dinitrobenzo[1,2,5]thiadiazole (2). Synthesized by the method of ref. 19. Yield 11.7 g (36%). M_p = 184–186 °C, lit. M_p = 198 °C.[18] 13C NMR ($CDCl_3$, 100 MHz, δ, ppm):

151.24, 144.81, 110.18. Found, %: C 18.62; Br 41.75; N 14.38. For $C_6Br_2N_4O_4S$ calculated, %: C 18.77; Br 41.62; N 14.59.

5,6-Dinitro-4,7-dithiophene-2-yl-benzo[1,2,5]thiadiazole (3). Synthesized by the method of ref. 19. Yield 5.4 g (62%). M_p = 260–261 °C, lit. M_p = 259–260 °C.[18] 1H NMR ($CDCl_3$, 400 MHz, δ, ppm): 7.73 (d, J = 6.3 Hz, 2H), 7.51 (d, J = 4.9 Hz, 2H), 7.23 (t, J = 5.0 Hz, 2H). 13C NMR (CDCl3, 100 MHz, δ, ppm): 179.43, 136.05, 132.48, 131.30, 130.84, 127.87, 124.11. Found, %: C 43.11; H 1.44; N 14.24. For $C_{14}H_6N_4O_4S_3$ calculated, %: C 43.07; H 1.55; N 14.35.

4,7-Dithiophene-2-yl-benzo[1,2,5]thiadiazole-5,6-diamine (4). Synthesized by the method of ref. 19. Yield 2.2 g (71%). M_p = 219–220 °C, lit. M_p = 239–240 °C.[20] 1H NMR ($CDCl_3$, 400 MHz, δ, ppm): 7.55 (d, J = 6.0 Hz, 2H), 7.36 (d, J = 3.4 Hz, 2H), 7.24 (t, J = 3.6 Hz, 2H), 4.38 (s, 4H). Found, %: C 50.80; H 3.00; N 17.06. For $C_{14}H_{10}N_4S_3$ calculated, %: C 50.89; H 3.05; N 16.95.

4,9-Bis-(thiophene-2-yl)-6,7-di-(2-ethylhexyl)-[1,2,5]thiadiazole-[3,4-*g*]quinoxaline (5). In a three-necked 250 mL flask equipped with a reflux condenser, a thermometer, the introduction of argon and a magnetic stirrer, 2.80 g (10.52 mmol) **4** and 4.7 g (10.52 mmol) 1,2-bis-(5-octylthiophene-2-yl)ethane-1,2-dione and 200 mL of $CHCl_3$ and CH_3OH (9 : 1) were placed and stirred at room temperature in a stream of argon for 48 h, then the solvent was evaporated on a rotary evaporator. Yield 2.1 g (67%). M_p = 111–113 °C. 1H NMR ($CDCl_3$, 400 MHz, δ, ppm): 7.82 (d, J = 4.2 Hz, 2H), 7.41 (d, J = 2.4 Hz, 2H), 7.17 (t, J = 3.6 Hz, 2H), 3.03 (d, J = 6.9 Hz, 4H), 2.28 (t, J = 5.7 Hz, 2H), 1.48–1.31 (m, 16H), 0.97–0.87 (m, 12H). Found, %: C 66.42; H 6.83; N 9.82. For $C_{32}H_{40}N_4S_3$ calculated, %: C 66.63; H 6.99; N 9.71.

4,9-Bis-(5-bromothiophene-2-yl)-6,7-di-(2-ethylhexyl)-[1,2,5]-thiadiazole[3,4-*g*]quinoxaline (6). In a three-necked 50 mL flask equipped with a reflux condenser, the introduction of argon with a magnetic stirrer, 1.8 g (3.69 mmol) 4,7-bis-(5-bromothiophene-2-yl)-benzo[1,2,5]thiadiazole-5,6-diamine, 2.08 g (7.37 mmol) 5,10-diethyltetradecane-7,8-dione and 110 mL of a mixture of $CHCl_3$/CH_3OH (9 : 1) were placed. The mixture was stirred at room temperature for 48 h, after which the solvent was evaporated on a rotary evaporator. The product was purified by column chromatography (silica gel, hexane : chloroform = 3 : 1). Yield 1.6 g (60%) of dark-blue crystals. M_p = 122–123 °C. 1H NMR ($CDCl_3$, 400 MHz, δ, ppm): 8.79 (d, J = 4.2 Hz, 2H), 7.17 (d, J = 4.2 Hz, 2H), 3.01 (d, J = 6.9 Hz, 4H), 2.26 (t, J = 5.7 Hz, 2H), 1.49–1.30 (m, 16H), 0.98–0.87 (m, 12H). Found, %: C 52.00; H 5.16; Br 21.95; N 7.45. For $C_{32}H_{38}Br_2N_4S_3$ calculated, %: C 52.32; H 5.21; Br 21.76; N 7.63.

2,6-Bis-trimethylstannyl-4,8-didodecyloxybenzo[1,2-*b*;4,5-*b*′]-dithiophene (7). Synthesized by analogy to ref. 21. Yield 7.1 g (90%). M_p = 48–50 °C. 1H NMR ($CDCl_3$, 400 MHz, δ, ppm): 7.50 (t, J = 14.1 Hz, 2H), 4.29 (t, J = 6.5 Hz, 4H), 1.88 (m, 4H), 1.60–1.53 (m, 4H), 1.40–1.24 (m, 32H), 0.88 (t, J = 6.8 Hz, 6H), 0.44 (t, J = 27.7 Hz, 18H). Found, %: C 53.98; H 8.03; S 7.24. For $C_{40}H_{70}O_2S_2Sn_2$ calculated, %: C 54.31; H 7.98; S 7.25.

Copolymer P. In a 25 mL three-necked flask equipped with a reflux condenser and magnetic stirrer, 0.7311 g (0.8265 mmol) of 2,6-bis-trimethylstannyl-4,8-didodecyloxybenzo[1,2-*b*;4,5-*b*′]-dithiophene (7) and 4,9-bis-(5-bromothiophene-2-yl)-6,7-di-(2-ethylhexyl)-[1,2,5]thiadiazolo[3,4-*g*]quinoxaline (**6**) as monomers and 0.065 g (0.056 mmol) $Pd(Ph_3P)_4$ were placed in a stream of argon and 15 mL dry toluene and 2 mL dry DMF were added. The reaction mixture was stirred at 115 °C for 48 h under argon. The mixture was then cooled to room temperature and the product was poured into 200 mL methanol and filtered. The polymer was dissolved in chloroform and reprecipitated in methanol, then purified by extraction with methanol, hexane, and acetone in a Soxhlet apparatus and dried in a vacuum. Yield 65%. 1H NMR ($CDCl_3$, 400 MHz, δ, ppm): 9.38–8.75 (m, 2H), 7.91–6.47 (m, 4H), 4.54–3.70 (m, 4H), 3.42–2.87 (m, 4H), 2.73–0.24 (m, 76H).

Device fabrication and characterization

BHJ solar cell devices having structures of ITO/PEDOT:PSS/**P**:$PC_{60}BM$ or $PC_{70}BM$/Al, used to investigate the photovoltaic properties, were fabricated as follows. The indium tin oxide coated glass substrates were cleaned by stepwise sonication in detergent, deionized water and isopropyl alcohol and dried. As a buffer layer, the conductive polymer PEDOT:PSS (Baytron) was spin coated onto ITO coated glass substrates from the aqueous solution of PEDOT:PSS, followed by annealing at 110 °C for 20 min to remove the water. The thickness of the PEDOT:PSS was about 60 nm. Solutions of **P** (7 mg mL^{-1}) and fullerene derivatives *i.e.* $PC_{60}BM$ or $PC_{70}BM$ (7 mg mL^{-1}, 14 mg mL^{-1}, 21 mg mL^{-1} and 28 mg mL^{-1}) were prepared in THF and mixed by blending **P** and fullerene solutions in the required volume ratios to obtain weight ratios of 1 : 1, 1 : 2, 1 : 3 and 1 : 4 of **P** and PCBMs. The active layers were deposited by spin coating the blend solution at 1500 rpm for 30 s onto PEDOT:PSS layer and were immediately covered by a Petri-dish until dry. The films were then dried at 70 °C for 20 min before the deposition of the final aluminum (Al) electrode. The Al electrode was evaporated on the top of the active layer under a vacuum of less than 10^{-6} Torr through a shadow mask. The effective area of the devices was about 20 mm^2. The current–voltage (J–V) characteristics of the devices were obtained with a Keithley source measurement unit under AM 1.5 (100 mW cm^{-2}) illumination. The simulated AM 1.5 light was obtained using a xenon lamp coupled with an AM 1.5 optical filter. The incident photon to current conversion efficiency (IPCE) of the devices was recorded by illuminating the device through a monochromator coupled with a xenon lamp and the resulting photocurrent was measured with the Keithley electrometer under short circuit conditions. The IPCE was estimated at each wavelength using the following expression:

$$\mathrm{IPCE} = (1240 J_{sc}/\lambda P_{in})$$

where J_{sc} is the short circuit photocurrent, λ is the monochromatic wavelength of incident light and P_{in} is the incident light intensity per unit area.

Results and discussion

Synthesis and characterization of P

The syntheses of the copolymer **P** and intermediate compounds are shown in Scheme 1. The purity, composition and structure of which are confirmed by melting point, NMR spectroscopy and elemental analysis. Nitration of 4,7-dibromobenzo[1,2,5]-thiadiazole **1** by fuming nitric acid in 100% sulfuric acid yielded

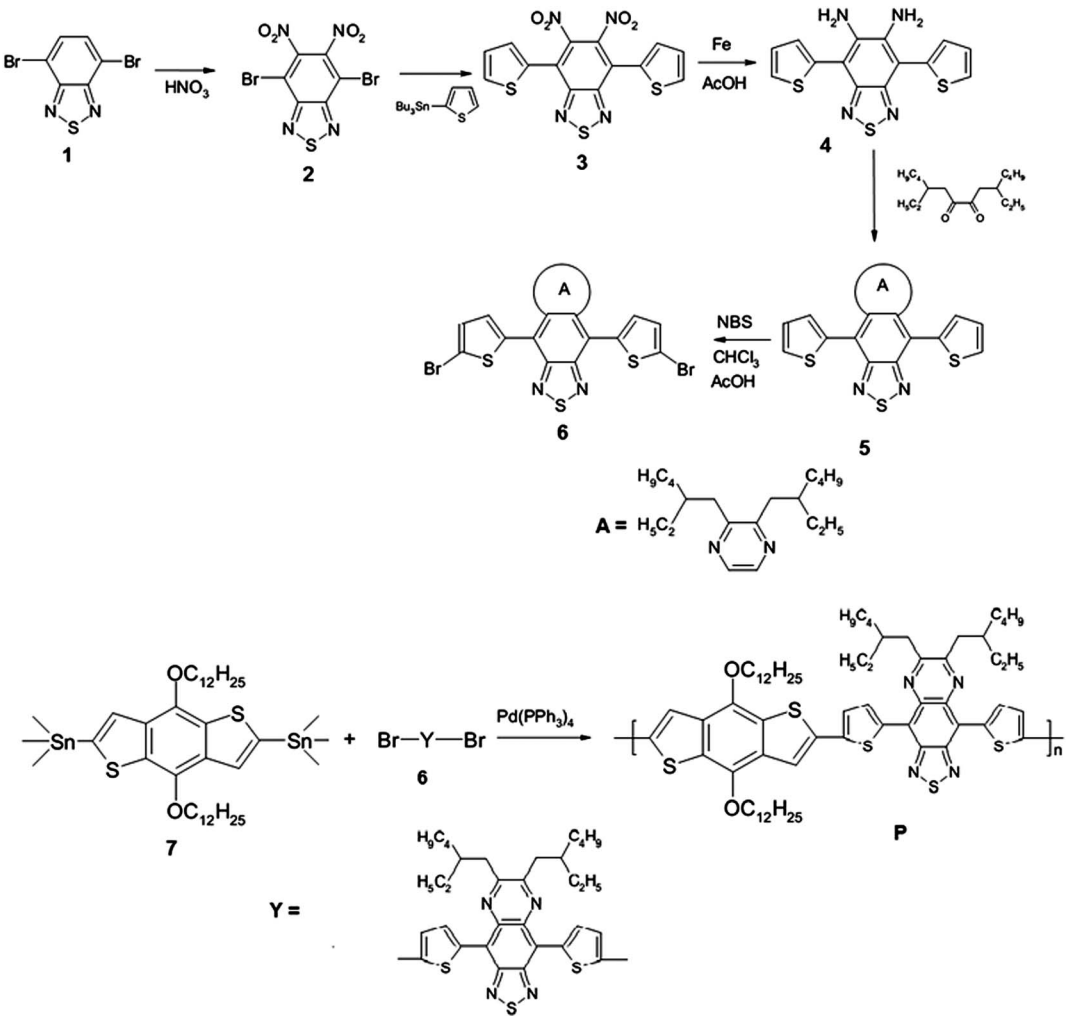

Scheme 1 Schematic routes for the synthesis of intermediate compounds to synthesise the copolymer **P** from compound **7**.

dinitroderivative **2**, which is then converted to the 5,6-dinitro-4,7-dithienyl-benzo[1,2,5]thiadiazole **3** by Stille cross-coupling in THF.[18] Reduction of **3** by iron powder in acetic acid resulted in 4,7-dithiophene-2-yl-benzo[1,2,5]thiadiazole-5,6-diamine **4**.[19]

By the interaction of 4,7-dithiophene-2-yl-benzo[1,2,5]thiadiazole-5,6-diamine **4** with 5,10-diethyltetradecane-7,8-dione, compound **5** was obtained, containing in its structure branched 2-ethylhexyl substituents, which give a high solubility to the condensed product.

By bromination of compound **5** with *N*-bromosuccinimide in THF at 0 °C, a new product, the heteroaromatic monomer 4,9-bis-(5-bromthiophene-2-yl)-6,7-di-(2-ethylhexyl)-[1,2,5]thiadiazole[3,4-*g*]quinoline **6** was obtained as a dark blue solid compound, the composition and structure of which are confirmed by elemental analysis and NMR spectroscopy.

The 1H NMR spectrum of compound **6** (Fig. 1) contains two doublet signals with $\delta_H = 8.79$ and 7.17 ppm with the coupling constant $J = 4.2$ Hz, belonging to protons of thiophene fragments, in the strong field area there are doublet, triplet, and two multiplet resonances, corresponding to protons of branched alkyl substituents.

Using the synthesized heteroaromatic thiophene-containing monomers, a low band gap copolymer **P** with the quinoid π-conjugation nature and a strict alternation of donor–acceptor

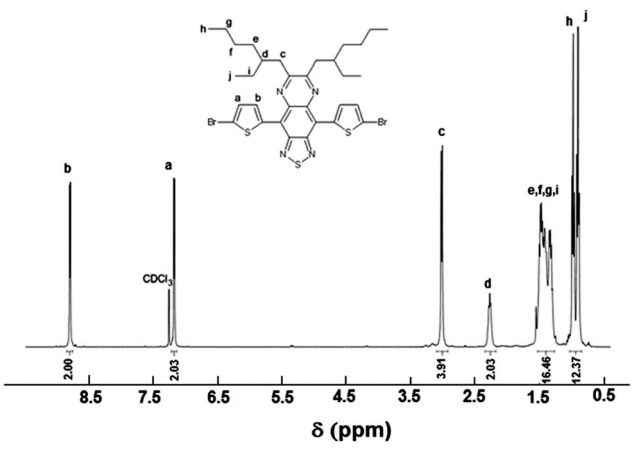

Fig. 1 1H NMR spectrum of 4,9-bis-(5-bromothiophene-2-yl)-6,7-di-(2-ethylhexyl)-[1,2,5]thiadiazolo[3,4-*g*]quinoxaline **6**.

units has been developed, obtained using the Stille cross-coupling reaction. Polycondensation was carried out under argon in a mixture of toluene and DMF at 115 °C for 48 h, using tetrakis-(triphenylphosphine)palladium (0) as a catalyst (see Scheme 1).

The resulting copolymer **P** was purified from the residual of metal catalyst, organotin and low molecular weight impurities by re-precipitation twice from solution in methanol and subsequent extraction with methanol, hexane and acetone. The yield of the desired high molecular mass product was 60–76%.

The composition and structure of the low band gap copolymer **P** were confirmed by 1H NMR spectroscopy. In particular, in the 1H NMR spectrum of copolymer **P** (Fig. 2), there are eight aromatic protons resonates in the field of $\delta_H = 8.43$–6.64 ppm. The protons signals of aliphatic fragments are located at intervals of $\delta_H = 4.79$–3.81, 3.20–2.68 and 2.28–0.63 ppm. The ratio of the integrated intensities of the aromatic and aliphatic protons for **P** corresponds to the expected pattern and confirms the structure of the elementary units of the macromolecule.

The average molecular weight and polydispersity of copolymer **P** determined by GPC (eluent-THF, standard-polystyrene) are 1.99×10^4 and 1.93, respectively. Copolymer **P** is soluble in common organic solvents such as DMF, *N*-methylpyrrolidone, chloroform, THF, *o*-dichlorobenzene. The glass transition temperature of copolymer **P** determined by TGA, is around 310 °C. $T_{5\%}$ values determined by TGA in air and in argon are in the range of 303 °C and 308 °C, respectively.

Optical and electrochemical properties

The photophysical characterization of the copolymer **P** was investigated by UV-visible–NIR absorption spectra of dilute THF solution and thin film spin coated on a quartz substrate. The normalized absorption spectra of **P** are shown in Fig. 3. The copolymer **P** showed two absorption peaks, which is a common feature of D–A type alternating copolymers.[22] The absorption peak in the shorter wavelength region having an absorption maximum at 448 nm is attributed to the π–π* transition of the conjugated backbone, while the absorption band in the longer wavelength region having an absorption peak at 744 nm corresponds to the intramolecular charge transfer from donor to acceptor unit present in the alternating copolymer **P**. The absorption bands in the film have peaks at 456 nm and 764 nm and are broader than those in solution, where two peaks are observed at 448 nm and 736 nm. The broadening of absorption peaks and redshift in absorption edge in the solid state indicates an increased π–π stacking form and stronger electronic interaction and aggregation between the individual polymer chains. The broadening and redshift in the absorption spectrum may also result from the increased polarizability of the polymer in thin film.[23] The optical bandgap (E_g^{opt}) estimated

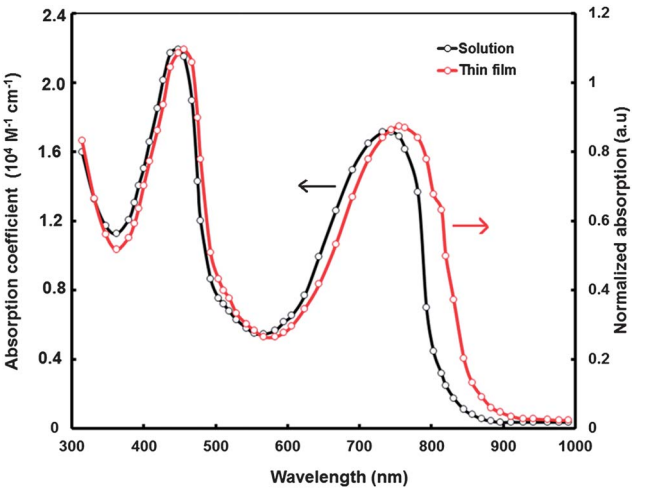

Fig. 3 Optical absorption spectra of copolymer **P** in THF solution and thin film (normalized absorption) cast from THF.

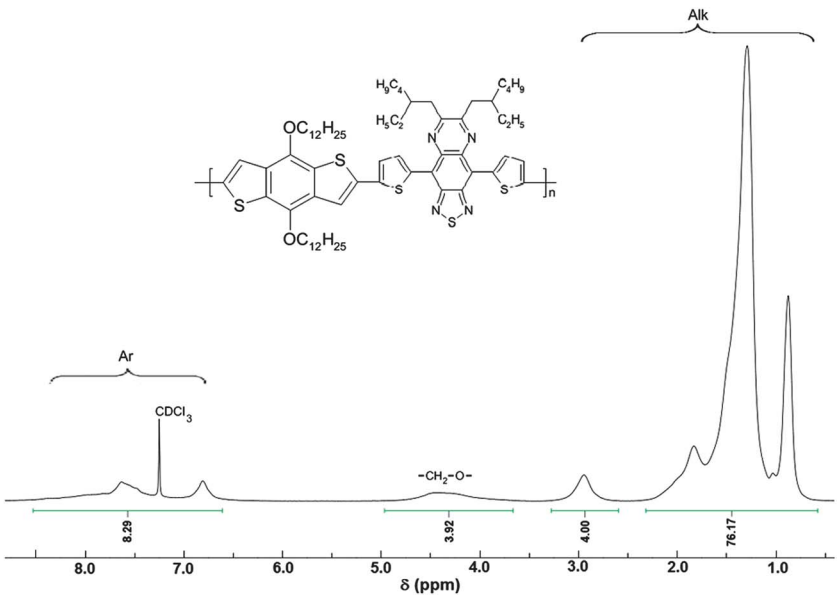

Fig. 2 1H NMR spectrum of low band gap copolymer **P** in $CDCl_3$.

from the onset (910 nm) of the **P** absorption spectrum in thin film is 1.38 eV, which is very close to the ideal bandgap of a donor for BHJ polymer solar cell application.[6a]

The HOMO and LUMO energy levels of the copolymer are essential to evaluate its suitability as donor component for the BHJ solar cell application. The HOMO and LUMO energy levels of **P** were estimated from the oxidation onset potential (E^{oxd}_{onset}) (0.45 V) and reduction oxidation potential (E^{red}_{onset}) (−1.03 V) observed in the cyclic voltammogram (Fig. 4), according to the following equations[24]

$$\text{HOMO} = -q(E^{ox}_{onset} + 4.71)\ \text{eV}$$

$$\text{LOMO} = -q(E^{red}_{onset} + 4.71)\ \text{eV}$$

where the potential unit is in V *vs.* Ag/Ag^{+}. The HOMO and LUMO levels of **P** were estimated to be −5.16 eV and −3.68 eV, respectively. The value of the HOMO level is similar to that observed for the D–A copolymer having BDT donor unit,[10m] since the HOMO level is governed by the donor unit in the alternating D–A copolymer. The energy difference between the LUMO of **P** and the LUMO level of fullerene derivatives is larger than the exciton binding energy, which is in the range of 0.25–0.30 eV for most of the organic materials. As a result, exciton dissociation would be possible. Moreover, the HOMO level of **P** is very close to the threshold HOMO energy level for air stable conjugated polymers, being estimated to be −5.2 eV.[25] The deep lying of the HOMO level of **P** may also be expected to yield a high value of V_{oc}, since the V_{oc} of a BHJ polymer solar cell is directly proportional to the difference between the HOMO level of donor and LUMO level of acceptor *i.e.* fullerene. The electrochemical band gap (E^{elec}_{g})of the copolymer **P** was calculated to be 1.48 eV, which is slightly higher than that of the optical band gap. The higher electrochemical band gap is a common phenomenon for conjugated polymers, because of the energy barrier of charge transfer at the electrodes during electrochemical measurements. Similarly, the HOMO level of **P** is −5.16 eV, which is approximately 1 eV higher lying than that of the HOMO level of fullerene derivatives. As a result, excitons generated in the fullerene may also be dissociated efficiently at the interface.[26]

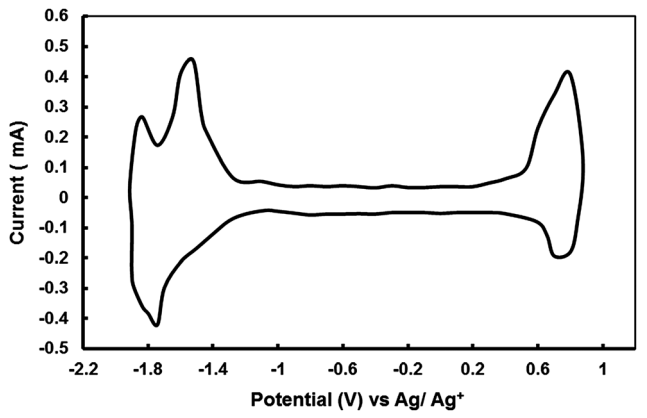

Fig. 4 Cyclic voltammogram of **P** film on glassy carbon electrode (0.1 mol L^{-1} Bu_4NPF_6, acetonitrile solution with the scan rate of 100 mV s^{-1}).

Theoretical calculations

In addition to the experimental measurements of HOMO and LUMO energy levels, we have investigated the structure of **P** theoretically within the framework of density functional theory (DFT) and time dependent density functional theory (TD-DFT). The monomers of **P** exhibit structural flexibility, which led us to design several stereoisomers as initial geometries for our calculations. The initial stereoisomers also include *cis*- and *trans*- configurations of the alkane units. The calculations have been performed employing the gradient corrected functional PBE[27] and the hybrid exchange correlation functional PBE0[28] (without adjustable parameters) of Perdew, Burke and Ernzerhof, as well as the hybrid functional of Becke, Lee, Yang, and Parr (B3LYP).[29] The long-range corrected functionals may outperform PBE0 on average only when the excitation energies are calibrated with per case linear corrections. We additionally provide calculations using the widely used B3LYP functional mainly as a reference and to facilitate comparison with the literature. We have used several stereoisomers for initial geometries' optimizations. The first round of calculations was performed employing the PBE functional. The resolution of the identity method was used for the treatment of two electron integrals. The TZVP basis set[30] which is of triple-ζ quality was used throughout. The resulting structures were further optimized using both the hybrid PBE0 and B3LYP functionals, using the same basis set and also taking into account solvent effects. The polarization continuum model (PCM)[31] was employed to account for effects from solute–solvent interactions. The TD-DFT excited state calculations have been performed using the same functionals on the corresponding ground state structures. In each case we have calculated the optical gap with and without the presence of solvents. For solvent we have used tetrahydrofuran (THF) using the self-consistent reaction field solvent parameters as defined in the Gaussian 09 electronic structure package.[32] The first round of geometry optimization was performed using the Turbomole package.[33] All of the follow up calculations were performed using the Gaussian package.[32]

The stereoisomers for the monomers of **P** were optimized at the PBE/TZVP level of theory and were found to be nearly isoenergetic. This is to be expected for rotamers and *cis*/*trans* isomers. The maximum energy difference for each case does not exceed 70 meV (1.6 kcal mol^{-1}), with the *trans* isomers energetically lower. This energy difference can be considered as the largest vertical rotational barrier in the gas phase. Corresponding adiabatic values would of course be larger and would account for possible steric effects.

The PBE functional belongs to the generalized gradient approximation (GGA) family of functionals, which are known to underestimate the highest occupied molecular orbital (HOMO)–lowest unoccupied molecular orbital (LUMO) gap (HLG). We can see that the PBE functional systematically underestimates the HLG, compared to the experimental values, on average by about 0.65 eV.

The energetically lowest isomer was further optimized initially in the gas phase employing the hybrid functionals PBE0

and B3LYP. No significant structural differences arise from these optimizations which suggests that the PBE functional produces high quality structures. The iso-surfaces (isovalue = 0.02) of the HOMO and LUMO of **P** are shown in Fig. 5 and the estimated values of HOMO and LUMO levels, HOMO–LUMO gap and optical band gap are listed in Table 1. The HOMO of the **P** monomers is delocalized over the dithiophene, thiophenes and thiadiazolo-quinoxaline units of the structure as shown in Fig. 5a. Contributions to the HOMO from the alkane groups are negligible. The LUMO is highly localized on the thiadiazolo-quinoxaline, however with significant contributions from the linking thiophenes. The values of the HOMO and LUMO energy levels, HOMO–LUMO gap and optical band gap estimated from the DFT calculations are very close to our experimental values.

Electrical properties of copolymer P

We have investigated the electrical properties in the dark of the copolymer **P** to get information about its semiconducting nature. The current–voltage (*J–V*) characteristics of the device ITO/PEDOT:PSS/**P**/Al in the dark are shown in Fig. 6. The device showed a rectification effect in the dark when a positive potential is applied to the ITO/PEDOT:PSS electrode with respect to Al. Since the HOMO level of **P** is very close to the work function of PEPOT:PSS (−5.1 eV), the holes are easily injected from PEDOT:PSS into the HOMO level of **P** when a positive potential is applied to the ITO electrode and an Ohmic contact is formed at the ITO/PEDOT:PSS–**P** interface. However, the LUMO level of **P** is very far from the work function of the Al electrode (−4.2 eV), and forms a Schottky barrier for electron injection from the Al into the LUMO level of **P**. Therefore, the rectification effect observed is due to the formation of a Schottky barrier at Al–**P** interface and copolymer **P** behaves as a p-type semiconductor and can be used as an electron donor for the BHJ device.

Photovoltaic properties of BHJ solar cells

In BHJ polymer solar cells, the composition of donor and acceptor materials used in the BHJ active layer has a large effect on the PCE of the device, because there should be a balance between the absorbance and charge transport network of the BHJ active layer. When the acceptor content is too low, the electron transport ability is limited. Moreover, when the acceptor content is too high, the absorbance and hole transport ability will be decreased. Therefore, initially we have investigated the photovoltaic properties of the devices with different weight ratios of **P** and $PC_{60}BM$ or $PC_{70}BM$ (1 : 1, 1 : 2, 1 : 3 and 1 : 4). We found that the optimal D : A ratio for **P** and PCBM or PCBM based devices is 1 : 2. The photovoltaic properties of the copolymer **P** were investigated using solution processed BHJ solar cells with device structures of ITO/PEDOT:PSS/**P**:$PC_{60}BM$ or $PC_{70}BM$ (1 : 2 w/w)/Al. The blends **P**:$PC_{70}BM$ were processed from THF. The *J–V* characteristics of the devices prepared from **P**:$PC_{60}BM$ and **P**:$PC_{70}BM$ measured under the illumination of AM 1.5 (100 mW cm^{-2}) are shown in Fig. 7(a) and the photovoltaic parameters are summarized in Table 2. The photovoltaic device made from **P**:$PC_{60}BM$ as an active layer shows a PCE of 2.10% with a V_{oc} of 0.78 V, a J_{sc} of 6.21 mA cm^{-2}, and a FF of 0.43, while that made from **P**:$PC_{70}BM$ as an active layer shows a PCE of 3.26% with a V_{oc} of 0.76 V, a J_{sc} of 8.93 mA cm^{-2} and a FF of 0.48. The two photovoltaic devices prepared from $PC_{60}BM$ or $PC_{70}BM$ as electron acceptor show quite similar V_{oc} values. However, the J_{sc} value of the device made from **P**:$PC_{70}BM$ is greater than that of the device prepared from **P**:$PC_{60}BM$. This is attributed to the strong absorption of $PC_{70}BM$ as compared to $PC_{60}BM$, which leads to the generation of more excitons in the **P**:$PC_{70}BM$ blend as compared to the **P**:$PC_{60}BM$, resulting in the higher J_{sc}. The IPCE spectra of the BHJ polymer solar cells were measured under monochromatic illumination and are shown in Fig. 7(b). The shapes of the IPCE spectra of the devices are similar to the absorption spectra of their active layer used. This indicates that in the device based on **P**:$PC_{60}BM$, most of the absorbed photons of copolymer **P** contribute to the photocurrent, while in the case of the device based on **P**:$PC_{70}BM$, photons absorbed by both **P** and $PC_{70}BM$ contribute to the photocurrent.

For the **P**:$PC_{70}BM$ BHJ active layer, using THF as a processing solvent, only a moderate PCE of 3.26% was achieved with a J_{sc} of 8.93 mA cm^{-2}, since the J_{sc} generally depends upon the morphology of the active layer. The film morphology can be improved through several processing methods *i.e.* thermal annealing, solvent annealing and solvent additives. We have tried to improve the PCE of the BHJ solar cells based on **P**:$PC_{70}BM$ processed using a solvent additive, *i.e.* 3 vol% 1,8-diiodooctane (DIO) was added to the blend solution in THF. The *J–V* characteristics and the IPCE spectra of the device based on the blend processed from DIO/THF are shown in Fig. 7 and photovoltaic parameters are compiled in Table 2. It can be seen from Table 2 that the PCE has been increased up to 4.47% as compared to 3.26% for the device processed from THF. The improvement in the PCE is mainly due to the enhancement in the J_{sc} (10.98 mA cm^{-2}) and FF (0.55). The improvement in the J_{sc} and FF has been attributed to the increase in both the crystalline nature of the blend and its absorption profile. It can be seen from the IPCE spectrum (Fig. 7(b)) of the device based on **P**:$PC_{70}BM$ processed from DIO/THF, the broader and higher IPCE value for this device results in a higher value of J_{sc} compared to the device based on the blend processed from THF.

The XRD patterns of the **P**:$PC_{70}BM$ thin films processed with and without DIO are shown in Fig. 8. The decrease in the full

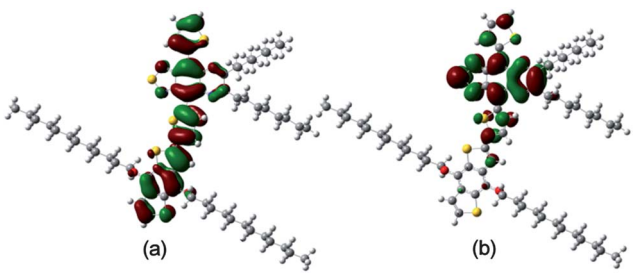

Fig. 5 Optimized geometry and calculated frontier molecular orbitals *i.e.* (a) HOMO and (b) LUMO for copolymer **P**.

Table 1 Calculated values of HOMO and LUMO energy levels, HOMO–LUMO gap and optical band gap from PBE0 and B3LYP models in gas phase and THF solvent

Medium		HOMO (eV)	LUMO (eV)	HL gap (eV)	Optical band gap (eV)
Gas	PBE0 model	−5.26	−3.24	2.02	—
	B3LYP model	−5.01	−3.27	1.74	—
THF	PBE0 model	−5.46	−3.33	2.13	1.66
	B3LYP model	−5.28	−3.45	1.83	1.54

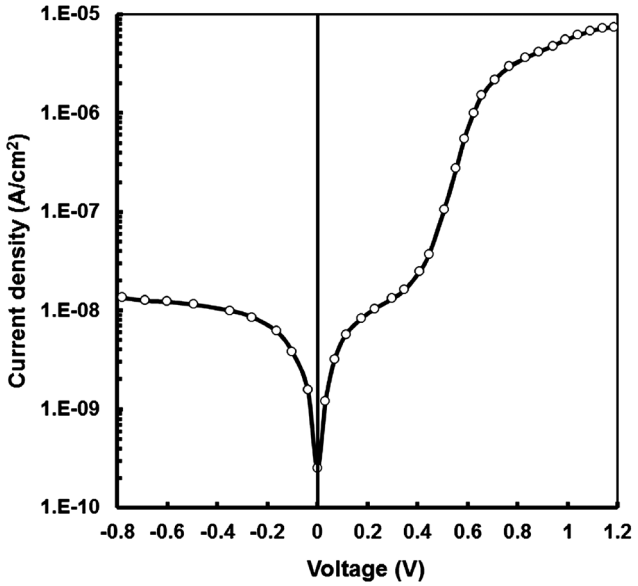

Fig. 6 Current–voltage characteristics of the ITO/PEDOT:PSS/**P**/Al in the dark at room temperature.

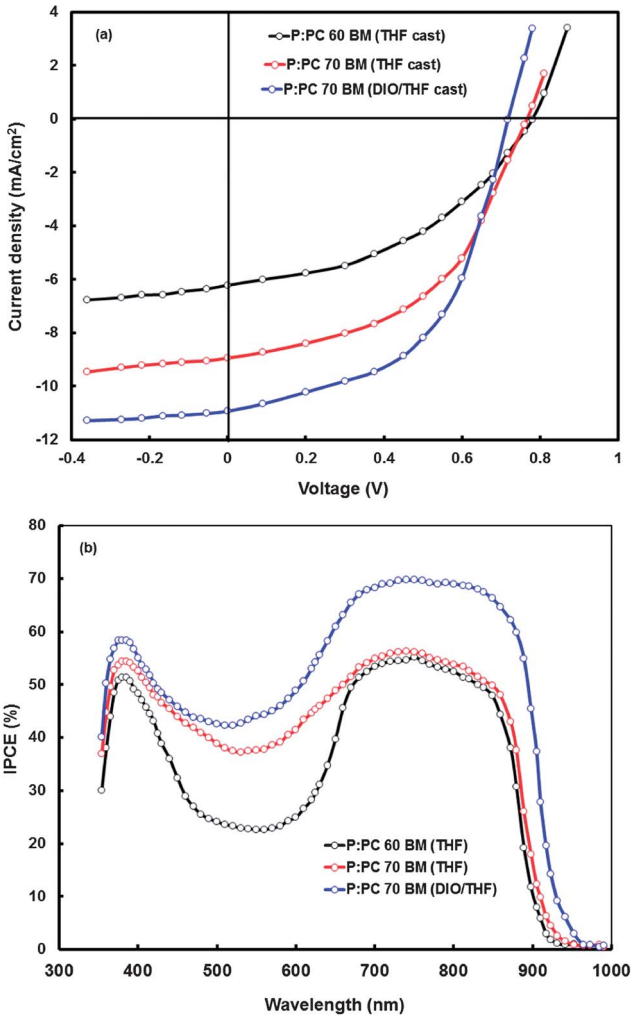

Fig. 7 (a) Current–voltage characteristics (b) IPCE spectra of the bulk heterojunction devices based on different blends under illumination (100 mW cm^{-2}).

width at half maxima of XRD patterns upon adding DIO indicated the strong improvement of the crystallinity of the copolymer, due to the high boiling point of DIO the active layer slowly dried, which assisted the formation of a self ordered structure in the blend. The blend film cast from the DIO/THF solution shows a more intense diffraction peak which indicates the higher order and crystallinity of the active layer. We believe that device performance improvement originates from two important contributions: an increased absorption in the active layer and increase in the charge carrier mobility. In order to understand how the addition of DIO affects the J_{sc}, the absorption spectra of thin films processed from THF and DIO/THF were measured and are shown in Fig. 9. The **P**:$PC_{70}BM$ blend film processed from the THF solution posses an absorption peak at 672 nm, which corresponds to the ICT from donor to acceptor in **P** and a shoulder around 835 nm, attributed to its crystalline π-stacking structure. The **P**:$PC_{70}BM$ blend film processed from the DIO/THF solution exhibited an almost similar absorption spectrum in the wavelength range 350–950 nm as cast from THF solution but an increased absorption coefficient and more pronounced shoulder peak which corresponds to the **P** in the blend. A significant redshift in the absorption peak corresponds to the ICT and pronounced shoulder peak indicate an enhanced conjugation length and more ordered structure of the copolymer. The enhanced optical absorption of the active layer results in the increased value of J_{sc}.

The balanced charge carrier mobility in the active layer is another important parameter that influences the J_{sc} of the organic solar cells. We measured the hole and electron mobilities of the blend films by the space charge limited current model with the ITO/PEDOT:PSS/blend/Au hole only and Al/blend/Al electron only devices, respectively, in the dark.[34] The hole mobility is 3.8×10^{-4} for DIO/THF blend film, which is about one order of magnitude larger than that prepared by THF solvent (2.4×10^{-5} cm^2 V^{-1} s^{-1}). The electron mobility also

Table 2 Photovoltaic parameters of the BHJ polymer solar cells

Blend	J_{sc} (mA cm^{-2})	V_{oc} (V)	FF	PCE (%)
P:PC$_{60}$BM[a]	6.21	0.78	0.43	2.10
P:PC$_{70}$BM[a]	8.93	0.76	0.48	3.26
P:PC$_{70}$BM[b]	10.98	0.74	0.55	4.47
P:PC$_{70}$BM[c]	11.47	0.72	0.62	5.12

[a] Cast from THF solvent. [b] Cast from DIO/THF solvent. [c] Cast from DIO/THF and DMSO doped PEDOT:PSS used as buffer layer.

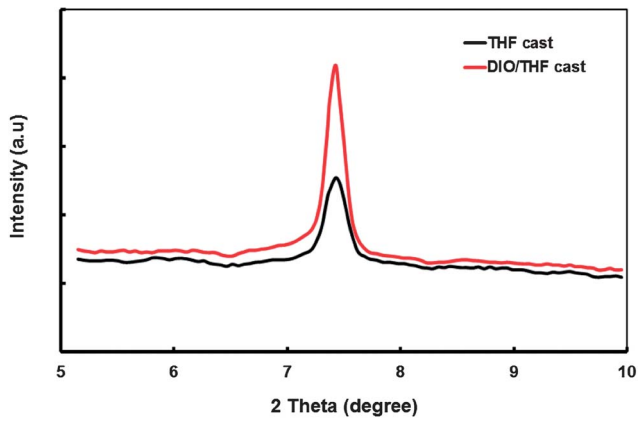

Fig. 8 XRD patterns of **P**:PC$_{70}$BM blend cast from THF and DIO/THF solvent.

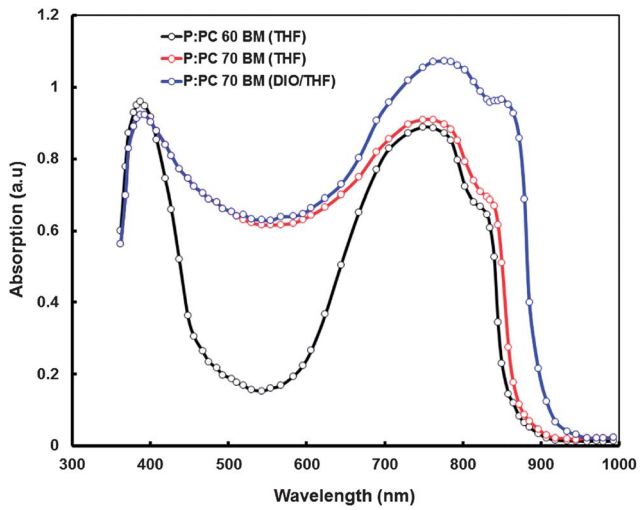

Fig. 9 Normalized optical absorption spectra of **P**:PC$_{60}$BM (THF cast), **P**:PC$_{70}$BM (THF cast) and **P**:PC$_{70}$BM (DIO/THF cast) blends in thin film form.

increased for the DIO/THF cast film but the degree of the increase is low, *i.e.* 2.36 × 10^{-3} cm^2 V^{-1} s^{-1} and 2.45 × 10^{-3} cm^2 V^{-1} s^{-1} for THF and DIO/THF cast films, respectively. The increase in the hole mobility reduces the ratio between electron and hole mobilities significantly in the active layer (98.3 to 6.45), and indicates a more balanced charge transport in the device based on the blend cast from DIO/THF solvent relative to that for the THF cast blend. The balanced charge transport within the active layer resulted in high J_{sc} and FF.

The AFM images for the THF and DIO/THF cast films are shown in Fig. 10. The surface roughness of the blend processed from THF solvent is about 2.45 nm but the blend processed from DIO/THF solvent shows a surface roughness of 4.31 nm. This is because the copolymer self organizes into the ordered structure and surface roughness increases after enough self organization time due to the high boiling point of DIO. The roughness is also considered to be the signature of polymer self organization.[35] The larger roughness of the blend film shows the higher ordered structure, which indicates reduced internal series resistance and more efficient charge separation in the organic solar cells. The film surface with higher roughness and nano-scaled texture also benefits the internal light scattering and enhances the light absorption.[36] In order to confirm this, the series resistances of BHJ devices processed from with and without DIO were calculated from the *J*–*V* characteristics of the devices around the voltage V_{oc}. The series resistance obtained for the device processed with DIO/THF is 4.28 Ω cm^2. This value is slightly smaller than 5.34 Ω cm^2, which is obtained for the device processed with THF. Moreover, the blend processed with DIO/THF solvent shows better phase separation than that for THF. The enhanced crystallinity of copolymer **P** decreases the solubility of the PC$_{70}$BM in it which results in a large scale of phase separation and continuous pathways. The better phase separation is favorable for efficient exciton dissociation and thereby provides continuous pathways for charge carrier transport.

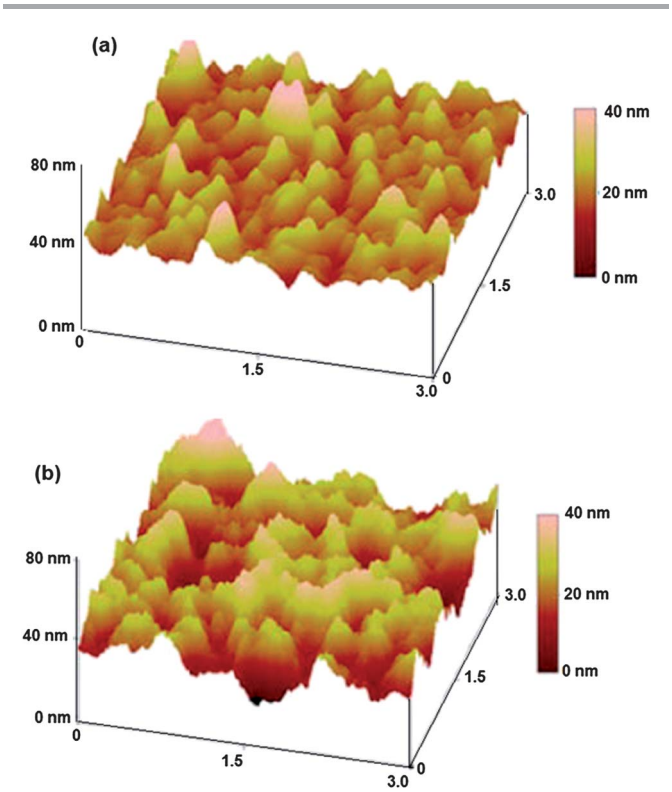

Fig. 10 AFM images of the **P**:PC$_{70}$BM blend cast from (a) THF and (b) DIO/THF solvent.

Effect of solvent addition in the PEDOT:PSS buffer layer

We have tried to improve the PCE of the solar cells, using the solvent doped PEDOT:PSS, as it was reported that the solvent doped PEDOT:PSS film showed superior conductivity.[37] We have used dimethyl sulfoxide (DMSO) as dopant which was added to the PEDOT:PSS directly and then the doped PEDOT:PSS was stirred for 30 min at room temperature. The doped PEDOT:PSS layer was deposited by spin coating method and than heated at 100 °C for 20 min on a hot plate in ambient conditions. In order to analyze the difference of these solvent doped PEDOT:PSS films, the electrical conductivity, morphology and optical properties of doped PEDOT:PSS were measured. We have used different concentrations of DMSO (by wt%) and found that 4 wt% was the optimal concentration to achieve the maximum PCE of the device. The ITO/PEDOT:PSS (doped DMSO)/**P**:$PC_{70}BM$ (DIO/THF cast)/Al device showed a PCE of 5.12%, with a J_{sc} of 11.47 mA cm^{-2}, V_{oc} of 0.72 and FF of 0.62. This shows that the increase in PCE is mainly due to the enhancements in the J_{sc} and FF. From the electrical conductivity measurement, we found that the sheet resistance of the PEDOT:PSS layer has been reduced upon the DMSO addition. From the AFM images, we found that following the addition of solvent in PEDOT:PSS, the film showed higher surface roughness. This is due to the fact that the amount of PEDOT:PSS molar ratio at the surface is increased and more PEDOT, which is a conductive material, will be clustered at the surface of the PEDOT:PSS film after the addition of DMSO. Moreover, this clustered phenomenon results in a decrease in the sheet resistance and an increase in the roughness of the surface. The reduced sheet resistance results in an improvement in charge transport towards the electrode. Moreover, the transmittance of the solvent added PEDOT:PSS film showed better transmittance over the whole wavelength region from 350 nm to 900 nm as compared to its pristine counterpart. The better transmission is beneficial to absorb more photons, which also leads to the enhancement in J_{sc}.

Conclusions

A low band gap D–A copolymer **P** based on BDT and DTQx units as electron donor and electron acceptor was synthesized and characterized through various characterization methods. This copolymer **P** exhibited broad absorption bands and appropriate HOMO and LUMO energy levels, and was employed as electron donor along with $PC_{60}BM$ or $PC_{70}BM$ as electron acceptor for BHJ polymer solar cells. The polymer solar cells based on **P**:$PC_{60}BM$ and **P**:$PC_{70}BM$ blends processed from the THF solvent showed PCE of 2.10% and 3.26%, respectively. The higher PCE for **P**:$PC_{70}BM$ blend as compared to **P**:$PC_{60}BM$ has been attributed to the stronger absorption of $PC_{70}BM$ in the visible region as compared to $PC_{60}BM$, leading to the photocurrent generation contribution from both **P** and $PC_{70}BM$. We have also demonstrated that DIO as solvent additive also enhances the PCE of the **P**:$PC_{70}BM$ based BHJ solar cell up to 4.47%. The use of solvent additive has a significant impact on the crystallinity and packing of **P** molecules and thus leads to a favorable phase separation morphology and increases the charge carrier mobility. The device with solvent added PEDOT:PSS layer showed further improvement up to 5.12% with a BHJ active layer **P**:$PC_{70}BM$ processed from DIO/THF solvent. The reduced sheet resistance of solvent added PEDOT:PSS layer leads to increased J_{sc} and FF. The reduction in sheet resistance of solvent added PEDOT:PSS layer was attributed to the morphology change, *i.e.* higher PEDOT to PSS molar ratio at the surface of PEDOT:PSS film. Furthermore, the better transmittance of the solvent added PEDOT:PSS layer as compared to pristine PEDOT:PSS may also result in an increase in the J_{sc} and PCE.

Acknowledgements

This work was supported by the Division of Chemistry and Material Science of the Russian Academy of Sciences (Basic Research Programs OKh-3 "Design and Study of Macromolecules and Macro-molecular Structures of New Generations", OKh-2 "Design of NewMetallic, Ceramic, Glass, Polymeric, and Composite Materials" and P-7 "Multifunctional materials for molecular electronics"). We are also thankful to Dr S. Biswas for providing the facilities to fabricate and characterize the devices.

References

1 (*a*) T. Yang, M. Wang, C. Duan, C. Hu, L. Hunag, J. Peng, F. Huang and X. Gong, *Energy Environ. Sci.*, 2012, **5**, 8208–8214; (*b*) G. Li, R. Zhu and Y. Yang, *Nat. Photonics*, 2012, **6**, 153–161; (*c*) G. Dennler, M. C. Scharber and C. J. Brabec, *Adv. Mater.*, 2009, **21**, 1323–1338; (*d*) Y. Y. Liang and L. P. Yu, *Polym. Rev.*, 2010, **50**, 454–473; (*e*) R. Sondergaard, M. Hosel, D. Angmo, T. T. Larsen-Olsen and F. C. Krebs, *Mater. Today*, 2012, **15**, 36–49; (*f*) S. H. Park, A. Roy, S. Beaupre, S. Cho, N. Coates, J. S. Moon, S. Moses, M. Leclerc, K. Lee and A. J. Heeger, *Nat. Photonics*, 2009, **2**, 297–302; (*g*) Z. He, C. Zhong, S. Su, M. Xu, H. Wu and Y. Cao, *Nat. Photonics*, 2012, **6**, 591–595; (*h*) X. Chen, B. Liu, Y. Zou, L. Xiao, X. Guo, Y. He and Y. Li, *J. Mater. Chem.*, 2012, **22**, 17724–17731; (*i*) C. Y. Chang, Y. J. Cheng, S. H. Hung, J. S. Wu, W. S. Kao, C. H. Lee and C. S. Hsu, *Adv. Mater.*, 2012, **24**, 549–553; (*j*) C. B. Nielsen, R. S. Ashraf, B. C. Schroeder, P. D'Angelo, S. E. Watkins, K. Song, T. D. Anthopoulos and I. McCulloch, *Chem. Commun.*, 2012, **48**, 5832–5834; (*k*) B. C. Thompson and J. M. J. Frechet, *Angew. Chem., Int. Ed.*, 2008, **47**, 58–77; (*l*) Y. J. Cheng, S. H. Yang and C. S. Hsu, *Chem. Rev.*, 2009, **109**, 5868–5923.

2 (*a*) G. Yu, J. Gao, J. C. Hummelen, F. Wudl and A. J. Heeger, *Science*, 1995, **270**, 1789–1791; (*b*) C. J. Brabec, N. S. Sariciftci and J. C. Hummelen, *Adv. Funct. Mater.*, 2001, **11**, 15–26.

3 (*a*) W. Ma, C. Yang, X. Gong, K. Lee and A. J. Heeger, *Adv. Funct. Mater.*, 2005, **15**, 1617–1622; (*b*) G. Li, V. Shrotriya, J. Huang, Y. Yao, T. Moriarty, K. Emery and Y. Yang, *Nat. Mater.*, 2005, **4**, 864–868; (*c*) J. Y. Kim, S. H. Kim, H. H. Lee, K. Lee, W. Ma, X. Gong and A. J. Heeger, *Adv. Mater.*, 2006, **18**, 572–576.

4 (*a*) Y. He, H. Y. Chen, J. Hou and Y. Li, *J. Am. Chem. Soc.*, 2010, **132**, 1377–1382; (*b*) G. Zhao, Y. He and Y. Li, *Adv.*

Mater., 2010, **22**, 4355–4358; (*c*) X. Guo, C. Cui, M. Zhang, L. Huo and Y. Li, *Energy Environ. Sci.*, 2012, **5**, 7943–7949.

5 M. C. Scharber, D. Muhlbacher, M. Koppe, P. Denk, C. Waldauf, A. J. Heeger and C. J. Brabec, *Adv. Mater.*, 2006, **18**, 789–794.

6 (*a*) N. Blouin, A. Michaud, D. Gendron, S. Wakim, E. Blair, N. P. Rodica, M. Belletete, G. Durocher, Y. Tao and M. Leclerc, *J. Am. Chem. Soc.*, 2008, **130**, 732–742; (*b*) H. Zhuo, L. Yang and W. You, *Macromolecules*, 2012, **45**, 607–632.

7 C. J. Brabec, A. Cravino, D. Meissner, N. S. Sariciftci, T. Fromherz, M. T. Rispens, L. Sanchez and J. C. Hummelen, *Adv. Funct. Mater.*, 2001, **11**, 374–380.

8 (*a*) E. E. Havinga, W. Hoeve and H. Wynberg, *Synth. Met.*, 1993, **55**, 299–306; (*b*) A. K. Agrawal and S. A. Jenekhe, *Macromolecules*, 1991, **24**, 6806–6808; (*c*) S. A. Jenekhe, L. Lu and M. M. Alam, *Macromolecules*, 2001, **34**, 7315–7324.

9 (*a*) C. M. Amb, S. Chen, K. R. Graham, J. Subbiah, C. E. Small, F. So and J. R. Reynolds, *J. Am. Chem. Soc.*, 2011, **133**, 10062–10065; (*b*) S. C. Price, A. C. Stuart, L. Q. Yang, H. X. Zhou and W. You, *J. Am. Chem. Soc.*, 2011, **133**, 4625–4631; (*c*) Z. C. He, C. M. Zhong, X. Huang, W. Y. Wong, H. B. Wu, L. W. Chen, S. J. Su and Y. Cao, *Adv. Mater.*, 2011, **23**, 4636–4637; (*d*) Y. Y. Liang, Z. Xu, J. B. Xia, S. T. Tsai, Y. Wu, G. Li, C. Ray and L. P. Yu, *Adv. Mater.*, 2010, **22**, E135–E136; (*e*) M. C. Scharber, M. Koppe, J. Gao, F. Cordella, M. A. Loi, P. Denk, M. Morana, H. J. Egelhaaf, K. Forberich, G. Dennler, R. Gaudiana, D. Waller, Z. Zhu, X. Shi and C. J. Brabec, *Adv. Mater.*, 2010, **22**, 367–370; (*f*) H. J. Son, L. Lu, W. Chen, T. Xu, T. Zheng, B. Carsten, J. Strzalka, S. B. Darling, L. X. Chen and L. Yu, *Adv. Mater.*, 2013, **25**, 838–843; (*g*) Y. Li, *Acc. Chem. Res.*, 2012, **45**, 723–733; (*h*) L. Huo, S. Zhang, X. Guo, F. Xu, Y. Li and J. Hou, *Angew. Chem., Int. Ed.*, 2011, **50**, 9697–9702.

10 (*a*) S. H. Park, A. Roy, S. Beaupre, S. Cho, N. Coates, J. S. Moon, D. Moses, M. Leclerc, K. Lee and A. J. Heeger, *Nat. Photonics*, 2009, **3**, 297–302; (*b*) S. C. Price, A. C. Stuart and W. You, *Macromolecules*, 2010, **42**, 4609–4612; (*c*) R. Qin, W. Li, C. Li, C. Du, C. Veit, H. F. Schleiermacer, M. Andersson, Z. Bo, Z. Liu, O. Inganas, U. Wuerfel and F. Zhang, *J. Am. Chem. Soc.*, 2008, **131**, 14612–14613; (*d*) H. Zhou, L. Yang, A. C. Stuart, S. C. Price, S. Liu and W. You, *Angew. Chem., Int. Ed.*, 2011, **50**, 2995–2998; (*e*) F. Zhang, E. Perzon, X. Wang, W. Mammo, M. R. Andersson and O. Inaganas, *Adv. Funct. Mater.*, 2005, **15**, 745–750; (*f*) M. M. Wienk, R. Turbiez, M. P. Struijk, M. Fonrodona and R. A. J. Janssen, *Appl. Phys. Lett.*, 2006, **88**, 153511–153513; (*g*) L. M. Campos, A. Tontcheva, S. Gunes, G. Sonmez, H. Neugebauer, N. S. Sariciftci and F. Wudl, *Chem. Mater.*, 2005, **17**, 4031–4033; (*h*) E. Zhou, J. Cong, S. Yamakawa, Q. Wei, M. Nakamura, K. Tajima, C. Yang and K. Hashimoto, *Macromolecules*, 2010, **43**, 2879; (*i*) M. M. Wienk, M. Turbiez, J. Gilot and R. A. Janssen, *Adv. Mater.*, 2008, **20**, 2556–2560; (*j*) J. C. Bijleveld, A. P. Zoombelt, S. G. J. Mathijssen, M. M. Wienk, M. Turbiez, D. M. Leeuw and R. A. J. Janssen, *J. Am. Chem. Soc.*, 2009, **131**, 16616–16617; (*k*) J. C. Bijleveld, V. S. Gevaerts, D. D. Nuzzo, M. Turbiez, S. G. Mathijssen, D. M. Leeuw and R. A. J. Janssen, *Adv. Mater.*, 2010, **22**, E242–E246; (*l*) C. Kanimozhi, P. Balraju, G. D. Sharma and S. Patil, *J. Phys. Chem. B*, 2010, **114**, 3095–3103; (*m*) T. Yamamoto, B. L. Lee, H. Kokubo, H. Kishida, K. Hirota, T. Wakabayashi and H. Okamoto, *Macromol. Rapid Commun.*, 2003, **24**, 440–443; (*n*) E. Wang, L. Hou, Z. Wang, S. Hellstrom, F. Zhang, O. Inganas and M. R. Andersson, *Adv. Mater.*, 2010, **22**, 5240–5244; (*o*) Y. Lee, T. P. Russell and W. H. Jo, *Org. Electron.*, 2010, **11**, 846–853; (*p*) Y. Lu, Z. Xiao, Y. Yuan, H. Wu, Z. An, Y. Hou, C. Gao and J. Huang, *J. Mater. Chem. A*, 2013, **1**, 630–637; (*q*) R. Duan, L. Ye, X. Guo, Y. Huang, P. Wang, S. Zhang, J. Zhang, L. Huo and J. Hou, *Macromolecules*, 2012, **45**, 3032–3038.

11 (*a*) Z. He, C. Zhong, X. Huang, W. Y. Wong, H. Wu, L. Chen, S. Su and Y. Cao, *Adv. Mater.*, 2011, **23**, 4636–4643; (*b*) T. Y. Chu, J. Lu, S. Beaupre, Y. Zhang, J. R. Pouliot, J. Zhou, A. Najari, M. Leclerc and Y. Tao, *Adv. Funct. Mater.*, 2012, **22**, 2345–2351; (*c*) Y. Huang, X. Guo, F. Liu, L. Huo, Y. Chen, T. P. Russell, C. C. Han, Y. Li and J. Hou, *Adv. Mater.*, 2012, **24**, 3383–3389; (*d*) Y. Liang, Z. Xu, J. Xia, S. T. Tsai, Y. Wu, G. Li, C. Ray and L. Yu, *Adv. Mater.*, 2010, **22**, E135–E138; (*e*) X. Li, C. H. Choy, L. Huo, F. Xie, W. E. I. Sha, B. Ding, X. Guo, Y. Li, J. Hou, J. You and Y. Yang, *Adv. Mater.*, 2012, **24**, 3046–3052.

12 H. Y. Chen, J. Hou, S. Zhang, Y. Liang, G. Yang, Y. Yang, L. Yu, Y. Wu and G. Li, *Nat. Photonics*, 2009, **3**, 649–653.

13 (*a*) Y. Lee, Y. M. Nam and W. H. Jo, *J. Mater. Chem.*, 2011, **21**, 8583–8590; (*b*) E. Wang, L. Hou, Z. Wang, S. Hellström, F. Zhang, O. Inganäs and M. R. Andersson, *Adv. Mater.*, 2010, **22**, 5240–5244; (*c*) E. Wang, L. Hou, Z. Wang, Z. Ma, S. Hellström, W. Zhuang, F. Zhang, O. Inganäs and M. R. Andersson, *Macromolecules*, 2011, **44**, 2067–2073; (*d*) J. Zhang, W. Cai, F. Huang, E. Wang, C. Zhong, S. Liu, M. Wang, C. Duan, T. Yang and Y. Cao, *Macromolecules*, 2011, **44**, 894–901; (*e*) A. Tsami, T. W. Bünnagel, T. Farrell, M. Scharber, S. A. Choulis, C. J. Brabecd and U. Scherf, *J. Mater. Chem.*, 2007, **17**, 1353–1355; (*f*) Y. Zhang, J. Y. Zou, H. L. Yip, K. S. Chen, D. F. Zeigler, Y. Sun and A. K. Y. Jen, *Chem. Mater.*, 2011, **23**, 2289–2291; (*g*) Y. Huang, M. Zhang, L. Ye, X. Guo, C. C. Han, Y. Li and J. Hou, *J. Mater. Chem.*, 2012, **22**, 5700–5705; (*h*) E. Zhou, J. Cong, K. Tajima and K. Hashimoto, *Chem. Mater.*, 2010, **22**, 4890–4895; (*i*) S. Li, Z. He, J. Yu, S. Chen, A. Zhong, H. Wu, C. Zhong, J. Qin and Z. Li, *J. Polym. Sci., Part A: Polym. Chem.*, 2012, **50**, 2819–2828.

14 (*a*) A. Gadisa, W. Mammo, L. M. Andersson, S. Admassie, F. Zhang, M. R. Andersson and O. Inganas, *Adv. Funct. Mater.*, 2007, **17**, 3836–3842; (*b*) E. Zhou, J. Z. Cong, K. Tajima and K. Hashimoto, *Chem. Mater.*, 2010, **22**, 4890–4895; (*c*) D. Kitazawa, N. Watanabe, S. Yamamoto and J. Tsukamoto, *Appl. Phys. Lett.*, 2009, **95**, 053701; (*d*) Z. He, C. Zhang, X. Xu, L. Zhang, L. Huang, J. Chen, H. Wu and Y. Cao, *Adv. Mater.*, 2011, **23**, 3086–3089; (*e*) X. Guo, M. Zhang, J. Tan, S. Zhang, L. Huo, W. Hu, Y. Li and J. Hou, *Adv. Mater.*, 2012, **24**, 6536–6541.

15 (*a*) X. Wang, E. Perzon, J. L. Delgado, P. Cruz and F. Zhang, *Appl. Phys. Lett.*, 2004, **85**, 5081–5083; (*b*) W. Wang, E. Perzon, F. Oswald, F. Langa, S. Admassie, M. R. Andersson and O. Inganäs, *Adv. Funct. Mater.*, 2005, **15**, 1665–1670; (*c*) H. Yi, R. G. Johnson, A. Iraqi, D. Mohamad, R. Royce and D. G. Lidzey, *Macromol. Rapid Commun.*, 2008, **29**, 1804–180.

16 (*a*) C. Winder and N. S. Sariciftci, *J. Mater. Chem.*, 2004, **14**, 1077–1086; (*b*) E. Bundgaard and F. C. Krebs, *Sol. Energy Mater. Sol. Cells*, 2007, **91**, 954–985.

17 C. Chen, Y.-H. Chen, C. C. Liu, Y. C. Chien, S. W. Chou and T. Chou, *Chem. Mater.*, 2012, **24**, 4766–4772.

18 (*a*) W. Lee, H. Choi, S. Hwang, J. Y. Kim and H. Y. Woo, *Chem.–Eur. J.*, 2012, **18**, 2551–2558; (*b*) P. Ding, C. C. Chu, B. Liu, B. Peng, Y. Zou, Y. He, K. Zhou and C. S. Hsu, *Macromol. Chem. Phys.*, 2010, **211**, 2555–2561.

19 E. Perzon, X. Wang, S. Admassie, O. Inganäs and M. R. Andersson, *Polymer*, 2006, **47**, 4261–4268.

20 M. Karikomi, C. Kitamura, S. Tanaka and Y. Yamashita, *J. Am. Chem. Soc.*, 1995, **117**, 6791–6792.

21 Y. Liang, D. Feng, Y. Wu, S. T. Tsai, G. Li, C. Ray and L. Yu, *J. Am. Chem. Soc.*, 2009, **131**(22), 7792–7799.

22 (*a*) C. L. Liu, J. H. Tsai, W. Y. Lee, W. D. Chen and S. A. Jenekhe, *Macromolecules*, 2008, **41**, 6952–6959; (*b*) J. E. Carlé, J. W. Andreasen, M. Jørgensen and F. C. Krebs, *Sol. Energy Mater. Sol. Cells*, 2010, **94**, 774–780; (*c*) L. Chen, D. Deng, Y. Nan, M. Shi, P. K. L. Chan and H. Chen, *J. Phys. Chem. C*, 2011, **115**, 11282–11292.

23 (*a*) Y. L. Shang, Y. Q. Wen, S. L. Li, S. X. Du, X. B. He, L. Cai, Y. L. Li, L. M. Yang, H. J. Gao and Y. Song, *J. Am. Chem. Soc.*, 2007, **129**, 11674–11675; (*b*) S. C. Price, A. C. Stuart and W. You, *Macromolecules*, 2010, **43**, 4609–4612.

24 J. Hou, Z. A. Tan, Y. Yan, Y. He, C. Yang and Y. Li, *J. Am. Chem. Soc.*, 2006, **128**, 4911–4916.

25 (*a*) B. C. Thompson, Y. G. Kim and J. R. Reynolds, *Macromolecules*, 2005, **38**, 5359–5362; (*b*) D. M. D. Leeuw, M. M. J. Simenon, A. R. Brown and R. E. F. Einerhand, *Synth. Met.*, 1997, **87**, 53–59.

26 G. Ren, C. W. Schlenker, E. Ahmed, S. Subramaniyan, S. Olthof, A. Kahn, D. S. Ginger and S. A. Jenekhe, *Adv. Funct. Mater.*, 2013, **23**, 1238–1249.

27 J. P. Perdew, K. Burke and M. Ernzerhof, *Phys. Rev. Lett.*, 1996, **77**, 3865–3868.

28 C. Adamo and V. Barone, *J. Chem. Phys.*, 1999, **110**, 6158–6169.

29 (*a*) A. D. Becke, *J. Chem. Phys.*, 1993, **98**, 5648–5652; (*b*) C. Lee, W. Yang and R. G. Parr, *Phys. Rev. B*, 1988, **37**, 785–89.

30 A. Schäfer, C. Huber and R. Ahlrichs, *J. Chem. Phys.*, 1994, **100**, 5829.

31 G. Scalmani and M. J. Frisch, *J. Chem. Phys.*, 2010, **132**, 114110.

32 M. J. Frisch, G. W. Trucks, H. B. Schlegel, G. E. Scuseria, M. A. Robb, J. R. Cheeseman, G. Scalmani, V. Barone, B. Mennucci, G. A. Petersson, H. Nakatsuji, M. Caricato, X. Li, H. P. Hratchian, A. F. Izmaylov, J. Bloino, G. Zheng, J. L. Sonnenberg, M. Hada, M. Ehara, K. Toyota, R. Fukuda, J. Hasegawa, M. Ishida, T. Nakajima, Y. Honda, O. Kitao, H. Nakai, T. Vreven, J. A. Montgomery, Jr, J. E. Peralta, F. Ogliaro, M. Bearpark, J. J. Heyd, E. Brothers, K. N. Kudin, V. N. Staroverov, R. Kobayashi, J. Normand, K. Raghavachari, A. Rendell, J. C. Burant, S. S. Iyengar, J. Tomasi, M. Cossi, N. Rega, J. M. Millam, M. Klene, J. E. Knox, J. B. Cross, V. Bakken, C. Adamo, J. Jaramillo, R. Gomperts, R. E. Stratmann, O. Yazyev, A. J. Austin, R. Cammi, C. Pomelli, J. W. Ochterski, R. L. Martin, K. Morokuma, V. G. Zakrzewski, G. A. Voth, P. Salvador, J. J. Dannenberg, S. Dapprich, A. D. Daniels, Ö. Farkas, J. B. Foresman, J. V. Ortiz, J. Cioslowski and D. J. Fox, *Gaussian 03, revision C.01*, Gaussian, Inc., Wallingford CT, 2004.

33 *TURBOMOLE (version 5.6)*, Universitat Karlsruhe, 2000.

34 (*a*) C. Melzer, E. J. Koop, V. D. Mihailetchi and P. W. M. Blom, *Adv. Funct. Mater.*, 2004, **14**, 865–870; (*b*) V. D. Mihailetchi, L. J. A. Koster, P. W. M. Blom, C. Melzer, B. De Boer, J. K. J. VanDuren and R. A. J. Janssen, *Adv. Funct. Mater.*, 2005, **15**, 795–801.

35 (*a*) X. Yang, J. Loos, S. C. Veenstra, W. J. Verhees, M. M. Wienk, J. M. Kroon, M. A. J. Michels and R. A. J. Janssen, *Nano Lett.*, 2005, **5**, 579–583; (*b*) G. Li, V. Shrotriya, J. S. Hung, Y. Yao, T. Moriarty, K. Emery and Y. Yang, *Nat. Mater.*, 2005, **4**, 864–868.

36 Q. Peng, X. J. Liu, Y. C. Qin, D. Zhou and J. Xu, *J. Polym. Sci., Part A: Polym. Chem.*, 2011, **49**, 4458–4467.

37 (*a*) J. Huang, P. F. Miller, J. S. Wilson, A. J. deMello, J. C. de Mello and D. D. C. Bradley, *Adv. Funct. Mater.*, 2005, **15**, 290–295; (*b*) O. P. Dimitrieva, D. A. Grinko, Y. V. Noskov and A. A. Pud, *Synth. Met.*, 2009, **159**, 2237–2239.

